

Poly (Toluidine Blue) and Zirconia Nanoparticles Electrochemically Deposited at Gelatin-Multiwalled Carbon Nanotube Film for Amperometric H₂O₂ Sensor

Yu-Jung Chang, Arun Prakash Periasamy, and Shen-Ming Chen *

Department of Chemical Engineering and Biotechnology, National Taipei University of Technology, No.1, Section 3, Chung-Hsiao East Road, Taipei 106, Taiwan (ROC).

*E-mail: smchen78@ms15.hinet.net

Received: 1 July 2011 / Accepted: 14 August 2011 / Published: 1 September 2011

Herein we report the preparation of a novel nanocomposite film containing zirconia nanoparticles (ZrO₂ NPs), poly(toluidine blue O) (PTBO) and gelatin functionalized multiwalled carbon nanotubes (GCNT). Gelatin has been used as a dispersing agent to prepare stable dispersion of MWCNTs in doubly distilled water. The prepared GCNT aqueous dispersion possesses long-term storage stability at room temperature. ZrO₂ NPs and PTBO have been stepwise electrochemically deposited on the GCNT modified glassy carbon electrode (GCE) surface. The electrostatic interactions between the negatively charged ZrO₂ NPs and positively PTBO provide good stability to the composite film. GCNT present in the composite film endorse fast electron transfer process. The maximum surface coverage concentration (*I*) of PTBO was noticed at the nanocomposite film modified GCE, which is $0.324 \times 10^{-9} \text{ mol cm}^{-2}$. The reason for the high *I* value of PTBO at the composite film could be ascribed to the larger surface area of GCNT and ZrO₂ NPs. The composite film exhibits rapid electrocatalytic response in the linear H₂O₂ concentration range between 0.05 mM–0.25 mM, with a higher sensitivity of $82.13 \mu\text{A } \mu\text{M}^{-1} \text{ cm}^{-2}$. Moreover, the proposed nanocomposite film detects H₂O₂ present in antiseptic solutions in good linear range, which shows its good practical applicability.

Keywords: Electropolymerization, gelatin, multiwalled carbon nanotubes, zirconia nanoparticles, toluidine blue O, hydrogen peroxide

1. INTRODUCTION

The extensive applications of multiwalled carbon nanotube (MWCNT) composites in various fields such as biosensors [1], fuel cells [2], solar cells [3], photovoltaics [4], transistors [5], nanoscale devices [6], and other bio applications [7] have necessitated the quest for exploring fascinating materials with tunable properties. MWCNT composites with metal [8] and metal oxide nanoparticles

[9], and conducting polymers [10] have been widely employed for various biosensing applications. Especially, the utilization of MWCNT-conducting polymer composites in electrochemical sensors can be ascribed to the unique ability of the conducting polymers to channel the electron transport via pi electrons, the large surface area of MWCNT enabling proper electrical contact with the transducer surface, and the conducting polymer coating which acts as a transducer for converting physical phenomenon into electrical signals. Moreover, thin CNT networks can act as a conductive and transparent backbone structures for polymer coating which increases the electronic conductivity, and helps to achieve high sensitivity and selectivity towards specific analyte quantification [11].

Among various conducting polymers, phenothiazine dye based conducting polymers can be used for efficient electrode modification. They have the ability to mediate as well as to decrease the over potential of biomolecular oxidation/redox process, which is more versatile and it helps to overcome the interference and electrode surface fouling related problems. In particular, electropolymerized thin films of poly(toluidine blue O) (PTBO), has its unique applications in NADH sensing at very low over potential [12, 13]. Moreover, PTBO incorporated metal oxides [14] and MWCNTs [15] serve as a versatile matrix for NADH sensing at low over potentials.

Other than PTBO, zirconia nanoparticles (ZrO_2 NPs) have also been used to prepare ZrO_2 -MWCNT nanocomposites to study methanol oxidation [16]. Generally, ZrO_2 -MWCNT nanocomposites have been synthesized by hydrothermal routes [17] and chemical vapor deposition methods (CVD) [18]. However, introducing novel preparation methods with low cost and pollution free approaches involving diverse strategies can be useful in tailoring the properties of the ZrO_2 -MWCNT composites and it can extend their applications to a greater extent. Among various preparation methods, the electrochemical deposition methods [19, 20] are more advantageous, as they do not depend on any capping agents, tedious chemical or heat treatments, while the film thickness could be optimized directly by controlling the number of potential scan cycles, precursor and electrolyte concentrations and scan rates. Therefore, in this work we have followed the electrochemical synthesis route reported by Liu et al. [21] for electrochemically depositing thin film of ZrO_2 nanoparticles.

Hydrogen peroxide (H_2O_2) is an extensively studied compound of interest, and it is an essential component of plant tissues, and it is involved in the regulation of plant metabolism, defense, acclimatory processes and gene expression [22]. H_2O_2 has excellent oxidizing and antibacterial property, and it has been largely used in industries as an oxidizing agent [23], antibacterial agent [24] and bleaching agent [25]. The wide applications of H_2O_2 in diverse fields emphasized the demand to explore simple, cost-effective, easily portable tools with adaptable measurement protocols for H_2O_2 quantification. However, the important analytical requirements for rapid H_2O_2 monitoring such as high sensitivity, reliability and operational simplicity [26] were not achieved by the conventional approaches [27-29]. On the other hand, the electrochemical techniques produce highly sensitive H_2O_2 reduction with good selectivity.

In this work, we attempted to prepare a novel, conducting nanocomposite using gelatin dispersed MWCNTs (GCNTs), ZrO_2 NPs, and PTBO. Since it is difficult to disperse MWCNTs in aqueous solution, we used gelatin as a dispersing agent to prepare stable MWCNT dispersion as we reported before [30]. Hereafter, the term GCNT indicates gelatin dispersed MWCNT. As reported

earlier, the isoelectric point of ZrO_2 NPs is 7 [31], therefore ZrO_2 NPs are positively charged in acidic solutions and negatively charged in basic solution. So, first we deposited negatively charged ZrO_2 NPs on GCNT modified GCE. Then by using electropolymerization method, positively charged thin PTBO film was deposited on negatively charged ZrO_2 NPs. The electrostatic interactions between the oppositely charged ZrO_2 NPs and PTBO maintain the stability of the nanocomposite film. Moreover, the positively charged free $-\text{NH}_2$ groups present in the gelatin can hold the negatively charged ZrO_2 NPs, which can also provide good stability to the composite film. The prepared PTBO/ ZrO_2 /GCNT nanocomposite exhibits excellent electrocatalytic activity towards H_2O_2 present in lab and antiseptic samples in good linear concentration range.

2. EXPERIMENTAL

2.1. Reagents and Apparatus

Gelatin from porcine skin, type A was purchased from Sigma and used as received. MWCNTs with O.D. 10-15 nm, I.D. 2-6 nm, and length 0.1-10 μm was obtained from Aldrich and used without further purification. Zirconyl chloride octahydrate was purchased from Sigma-Aldrich. Toluidine blue O (TBO) was purchased from chroma-gesellschaft and used without further purification. 30 % H_2O_2 solution was obtained from Wako pure chemical industries, Ltd. and freshly prepared H_2O_2 solutions were prepared every day. The supporting electrolyte used for all experiments is 0.05 M pH 7 phosphate buffer solution (PBS), which is prepared by using 0.05 M Na_2HPO_4 and NaH_2PO_4 solutions. All the reagents used were of analytical grade and all aqueous solutions were prepared using doubly distilled water.

Electrochemical studies were performed in a conventional three electrode cell containing 4 ml of 0.05 M pH 7 PBS. Prior to each experiment, 0.05 M pH 7 PBS was deoxygenated by passing pre-purified N_2 gas for 10 min. Cyclic voltammetry (CV) studies were carried out using CHI 1205a work station. BAS GCE with an electrode surface area of 0.079 cm^2 was used as working electrode and Pt wire with 0.5 mm diameter was used as counter electrode. All the potentials were referred with respect to standard Ag/AgCl reference electrode. CHI-750 potentiostat was used for amperometric (i-t curve) studies. Surface morphological studies were carried out using Being Nano-instruments CSPM4000, atomic force microscope (AFM).

2.2. Fabrication of PTBO/ ZrO_2 /GCNT nanocomposite film modified GCE

2.2.1. Stepwise fabrication of GCNT and ZrO_2 NPs

GCNT used in this work was prepared according to the procedure reported elsewhere in the literature [30, 32]. 10 mg of MWCNT was added into 1 mg ml^{-1} of gelatin aqueous solution and ultra sonicated for 1 h to obtain a homogeneous, black dispersion containing 2 mg ml^{-1} of MWCNTs. The good stability of MWCNT in aqueous gelatin solution could be attributed to the strong interactions

between the hydrophobic amino acids chain of gelatin and hydrophobic side walls of MWCNTs [32]. GCE surface was polished well on a clean Buehler polishing cloth using 0.05 μm alumina slurry. Then the resulting clean GCE surface was washed several times with doubly distilled water, ultrasonicated for 10 min and finally dried at room temperature for few min. GCE was transferred to an electrochemical cell containing 4 ml of 0.2 M H_2SO_4 solution. To obtain stable voltammograms, about 10 consecutive cyclic voltammograms were performed in the potential range between 0.7 and -1.1 V. Finally, thus obtained clean GCE surface was washed several times with doubly distilled water and 10 μl of GCNT dispersion was drop casted and dried. ZrO_2 NPs were electrochemically deposited on the GCNT modified GCE as per the procedure reported in the literature [21]. Thus obtained GCNT/GCE was transferred to an electrochemical cell with 4ml of 0.05 M pH 7 PBS containing 5.0 mM ZrOCl_2 . As shown in fig. 1, 10 consecutive cyclic voltammograms were recorded in the potential range between 0.7 and -1.1 V vs. Ag/AgCl reference electrode at the scan rate of 20 mV s^{-1} to obtain stable voltammograms. The resulting ZrO_2 /GCNT film modified GCE was then rinsed with water and dried using N_2 .

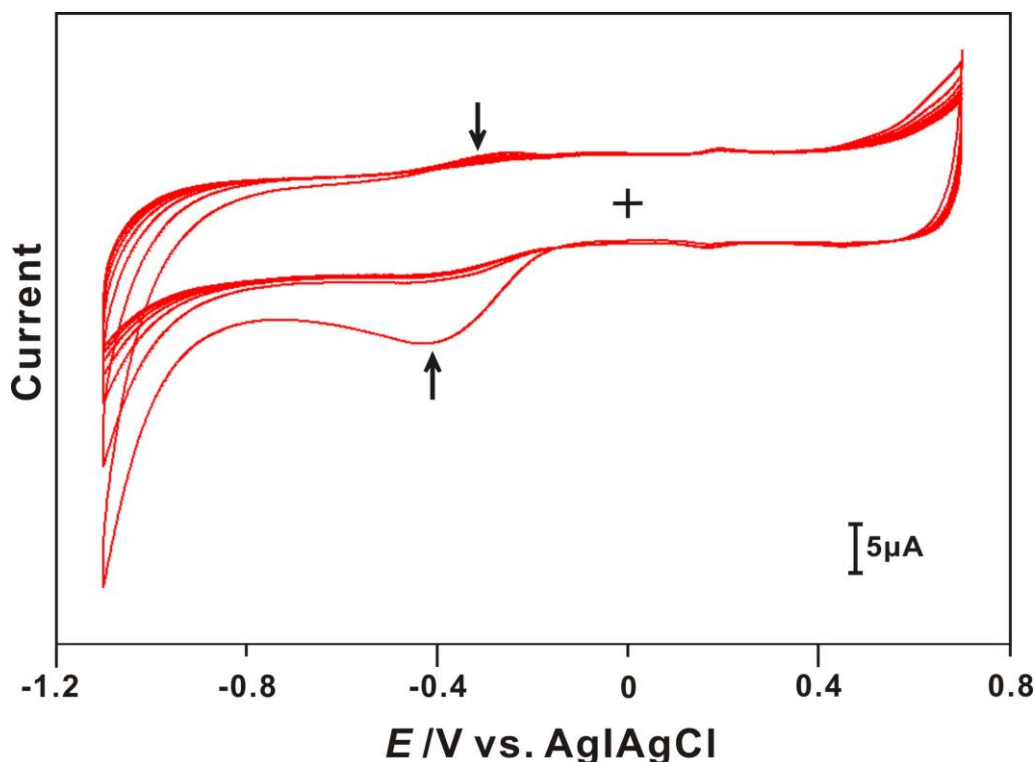


Figure 1. Consecutive cyclic voltammograms recorded at GCNT film modified GCE kept in 0.05 M pH 7 PBS containing 5.0 mM ZrOCl_2 . Scan rate: 0.1 V s^{-1} .

2.2.2. Electropolymerization of TBO at ZrO_2 /GCNT film modified GCE

The prepared ZrO_2 /GCNT film modified GCE was transferred to an electrochemical cell containing 4 ml of 0.3 mM TBO in 0.05 M pH 7 PBS. As shown in Fig. 2, consecutive 20 cyclic

voltammograms were performed in the potential range between -0.6 and 1 V at the scan rate of 100 mV s⁻¹.

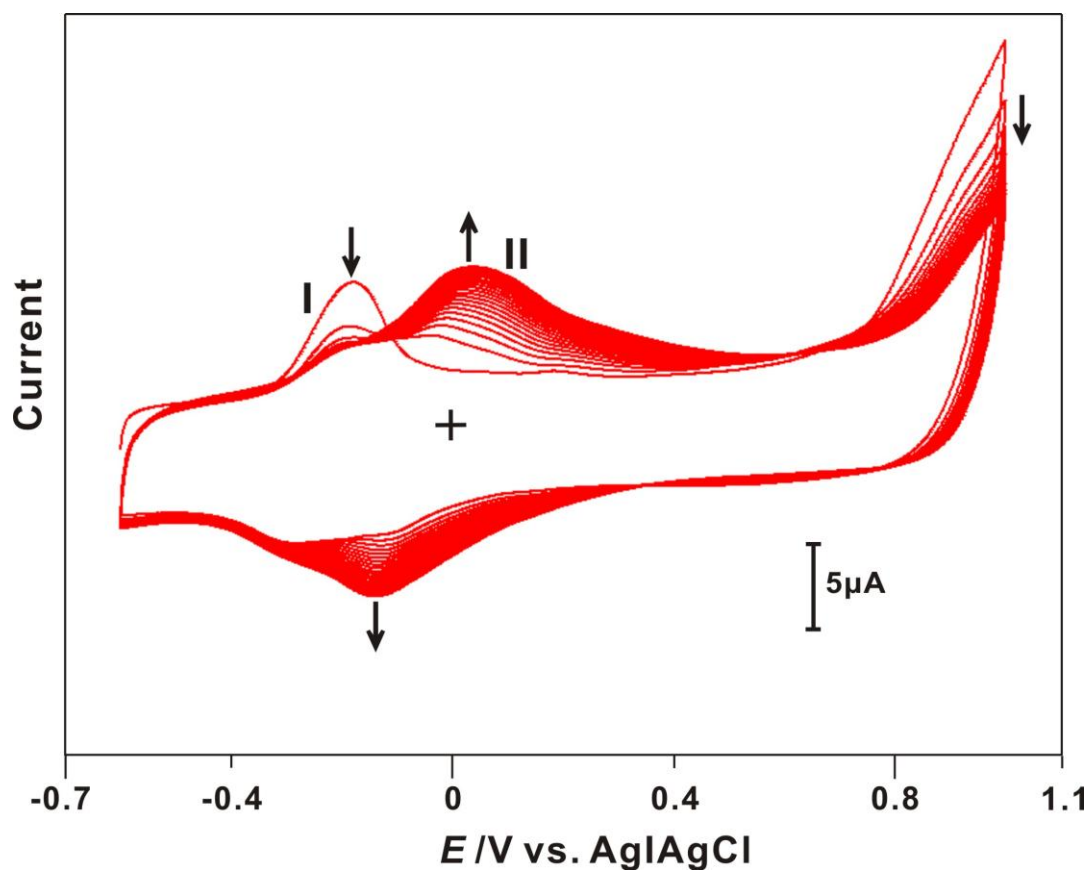
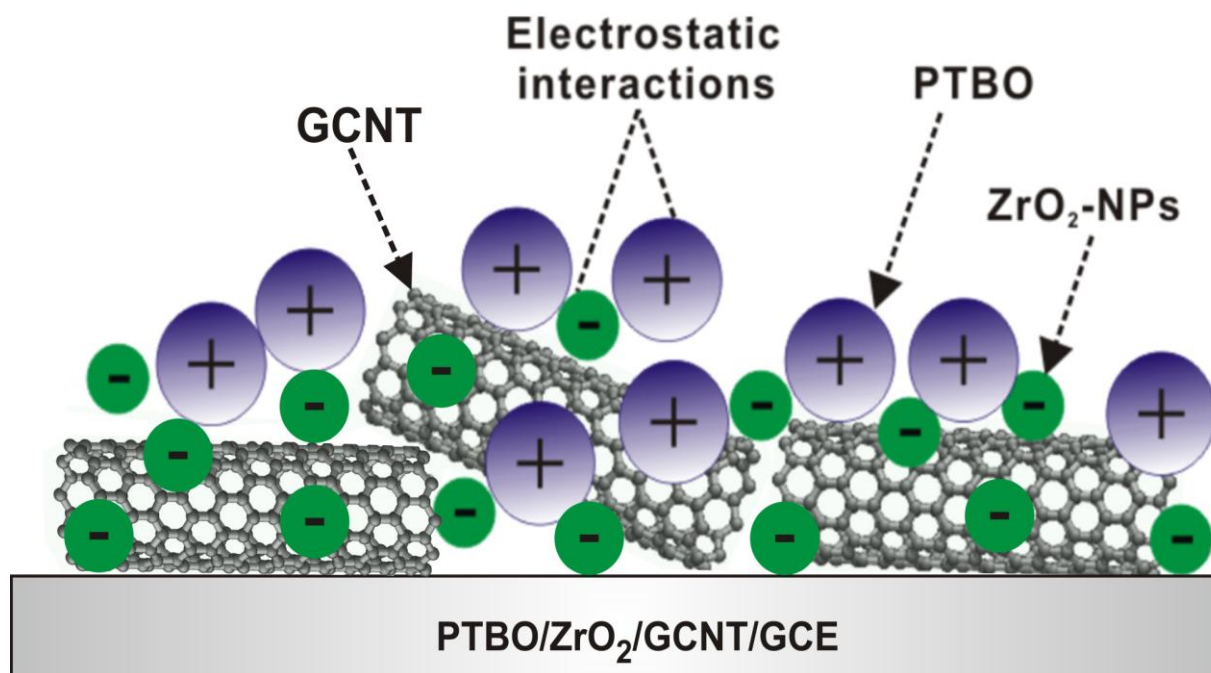


Figure 2. Consecutive 20 cyclic voltammograms recorded at ZrO₂/GCNT film modified GCE kept in N₂ saturated 0.05 M pH 7 PBS containing 0.3 mM of TBO. Scan rate: 0.1 V s⁻¹.

As a result of continuous CV potential cycling in the above mentioned potential range positively charged conducting PTBO was deposited on ZrO₂/GCNT film. As shown in Fig.2. during the forward scan, a large shoulder wave appears at -0.18 V followed by a small shoulder peak at + 0.04 V. TBO monomer oxidation occurs at a more positive oxidation potential of 0.8 V. In the reverse scan as a result of TBO reduction, a shoulder peak appears at -0.14 V. The redox peak currents of the TBO redox couple ($E_{pa} = +0.04$ and $E_{pc} = -0.14$ V) observed at a formal potential (E°) of -0.05 V increased continuously with increase in scan cycle numbers and the anodic and cathodic peak potentials shifted towards positive and negative directions, which confirmed the polymerization of PTBO at ZrO₂/GCNT surface. Moreover, in order to confirm whether the composite matrix containing GCNT and ZrO₂ NPs is efficient for PTBO deposition, we also performed the electrochemical deposition of PTBO comparatively at unmodified and ZrO₂ NPs modified electrode surfaces under similar experimental conditions (figure not shown). Compared with ZrO₂/GCNT composite matrix, unmodified and ZrO₂ matrices were not efficient for PTBO deposition, as they produced redox peaks with much smaller peak currents. On the other hand, the reason for the efficient PTBO deposition at ZrO₂/GCNT

composite matrix can be ascribed to the strong affinity between the positively charged PTBO and negatively charged ZrO_2 NPs. The schematic representation of the possible electrostatic interactions between PTBO and ZrO_2 NPs at PTBO/ ZrO_2 /GCNT/GCE is shown in scheme 1.



Scheme 1. Possible electrostatic interactions between ZrO_2 NPs and PTBO at PTBO/ ZrO_2 /GCNT film modified GCE.

3. RESULTS AND DISCUSSIONS

3.1. Investigation of electrochemical behavior of various film modified electrodes

To investigate the electrochemical behavior of various film modified electrodes, cyclic voltammograms were recorded at the scan rate of 50 mV s^{-1} in N_2 saturated 0.05 M pH 7 PBS in the potential range between 0.5 and -0.7 V as shown in Fig.1. It is obvious that no significant redox peaks were observed at only GCNT, ZrO_2 NPs and GCNTs/ ZrO_2 NPs modified GCEs. However, PTBO/ ZrO_2 /GCNT/GCE exhibits two well defined redox peaks (I and II) in this potential window. The $E^{\circ'}$ values of redox peaks I and II are -0.271 V and -0.06 V , respectively. As reported by Cai *et al.* the redox couple I correspond to the redox reaction of monomer units existing in PTBO film, while the redox couple II represents the redox reaction of the nitrogen bridges present in the polymer [12].

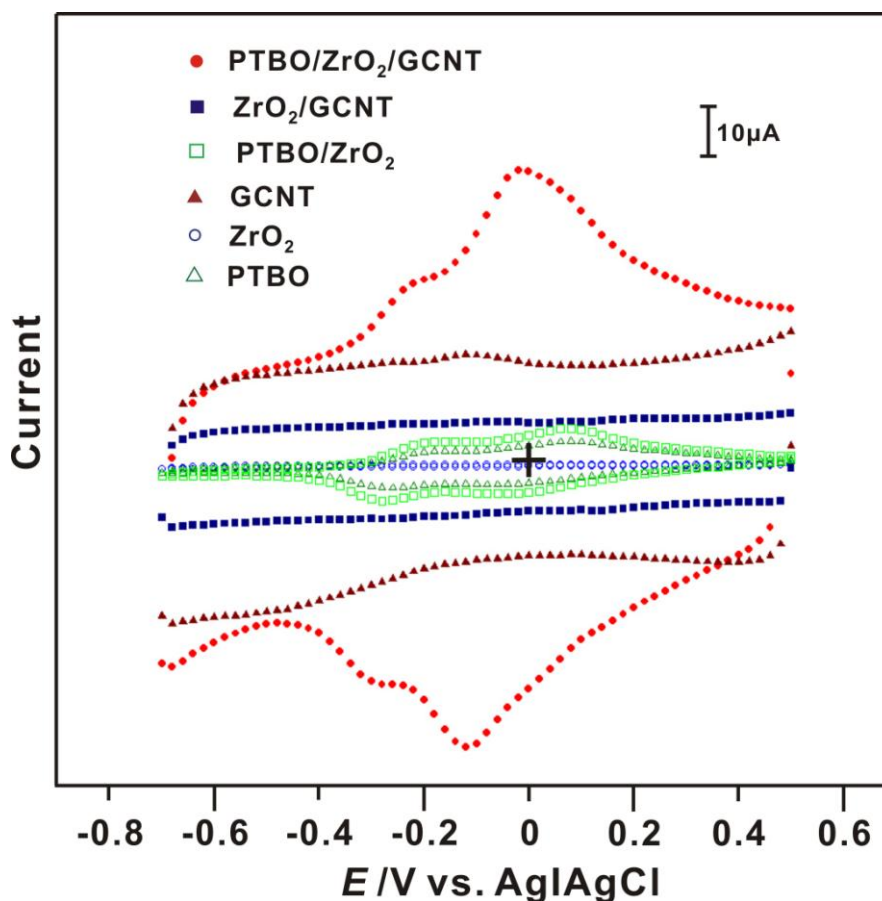


Figure 3. Cyclic voltammograms obtained at PTBO, ZrO₂, GCNT, PTBO/ZrO₂, ZrO₂/GCNT, and PTBO/ZrO₂/GCNT film modified GCEs in N₂ saturated 0.05 M pH 7 PBS at the scan rate of 50 mV s⁻¹.

The E° values of the PTBO redox couples I and II observed at PTBO/ZrO₂/GCNT/GCE are 66 and 41 mV positive than the E° values of the PTBO redox couples I and II at bare GCE electrode reported by Wang *et al.* [33] The reason for the shift in E° values towards positive potential may be ascribed to the interaction between positively charged PTBO and negatively charged ZrO₂ at GCNT surface. Moreover, comparing the redox peaks (I and II) observed at PTBO/ZrO₂/GCNT, PTBO and PTBO/ZrO₂ NPs modified GCEs it is obvious that PTBO and PTBO/ZrO₂ NPs exhibit similar redox peaks with much lesser peak currents. The enhanced redox peak currents observed at the PTBO/ZrO₂/GCNT/GCE validates the effective role and the ability of ZrO₂ NPs incorporated GCNT nanocomposite matrix to endorse the electron transfer of the TBO redox process.

3.2. Different scan rate studies

Fig. 4 shows the cyclic voltammograms recorded at PTBO/ZrO₂/GCNT/GCE in N₂ saturated 0.05 M pH 7 PBS at different scan rates. The PTBO/ZrO₂/GCNT nanocomposite film exhibits well defined redox peaks (I and II) at the scan rate 50 mV s⁻¹. Both these redox peaks exhibit a linear dependence on scan rates. The redox peaks currents and the peak potential separation (ΔE_p) increased

with increasing the scan rates between 100-500 mV s^{-1} , which confirmed the surface confined redox process. The linear dependence of I_{pc} of peaks I and II on different scan rates is shown in fig. 4 inset.

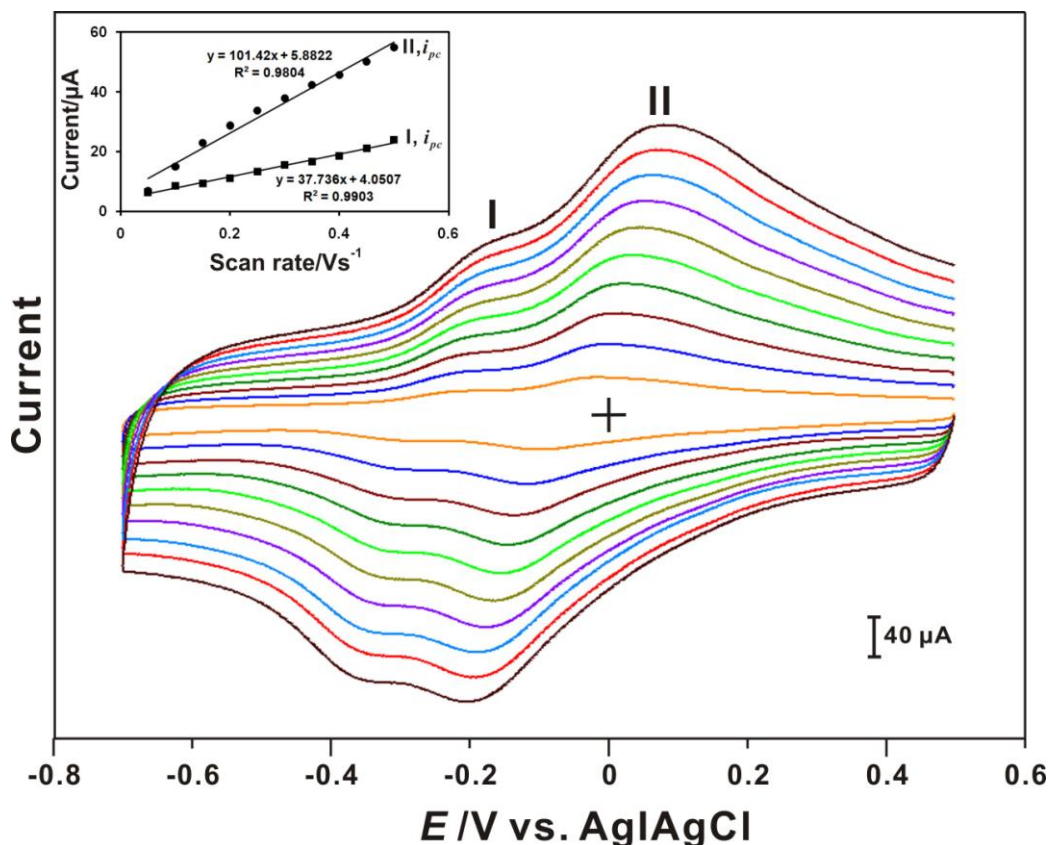


Figure 4. Cyclic voltammograms obtained at PTBO/ ZrO_2 /GCNT composite film modified GCE in N_2 saturated 0.05 M pH 7 PBS at different scan rates. The scan rates from inner to outer are: 50, 100, 150, 200, 250, 300, 350, 400, 450 and 500 mV s^{-1} . Inset shows the linear dependence of I_{pc} of the redox peaks I and II on scan rates (Vs^{-1}).

The surface coverage concentration (Γ) of PTBO on PTBO/ ZrO_2 /GCNT, unmodified and ZrO_2 NPs modified GCEs have been calculated and they are comparatively given in Table. 1. The Γ value has been calculated for peak II, since it corresponds to the polymer type reaction. The number of electrons involved in the TBO redox process is considered as two and the GCE surface area as 0.079 cm^2 .

From Table.1 it is evident that comparing all the above mentioned modified electrodes, maximum Γ value of $0.324 \times 10^{-9} \text{ mol cm}^{-2}$ is observed at PTBO/ ZrO_2 /GCNT modified GCE, validating the efficient deposition of PTBO at the nanocomposite film. Moreover, comparing the Γ values of PTBO/GCE with PTBO/ ZrO_2 /GCE, it is understandable that about 2.2 folds increase in Γ value is observed at the later, which can be attributed to the strong electrostatic interactions between PTBO and ZrO_2 NPs. Similarly, the Γ value of PTBO at the nanocomposite film is 2.3 fold higher than the Γ value of PTBO at PTBO/ ZrO_2 film, which shows the inherent role played by GCNT at the former in facilitating the PTBO deposition.

Table 1. Comparison of surface coverage concentration (Γ) values of PTBO at various electrodes

Type of electrode	Surface coverage concentration (Γ) values (nmol cm ⁻²)
	Peak-II
^a PTBO/GCE	0.066
^a PTBO/ZrO ₂ /GCE	0.143
^a PTBO/ZrO ₂ /GCNT	0.324

^a CV studies were done at all the above mentioned modified electrodes in 0.05 M pH 7 PBS at 50 mV s⁻¹ scan rate.

3.3. Influence of pH

Fig. 5 shows the effect of pH on PTBO/ZrO₂/GCNT modified GCE in different buffer solutions in the pH range between 1 and 13. Well defined redox peaks (I and II) were observed in the investigated wide pH range, and the redox couples are reproducible when the modified GCE was transferred from one pH solution to the other.

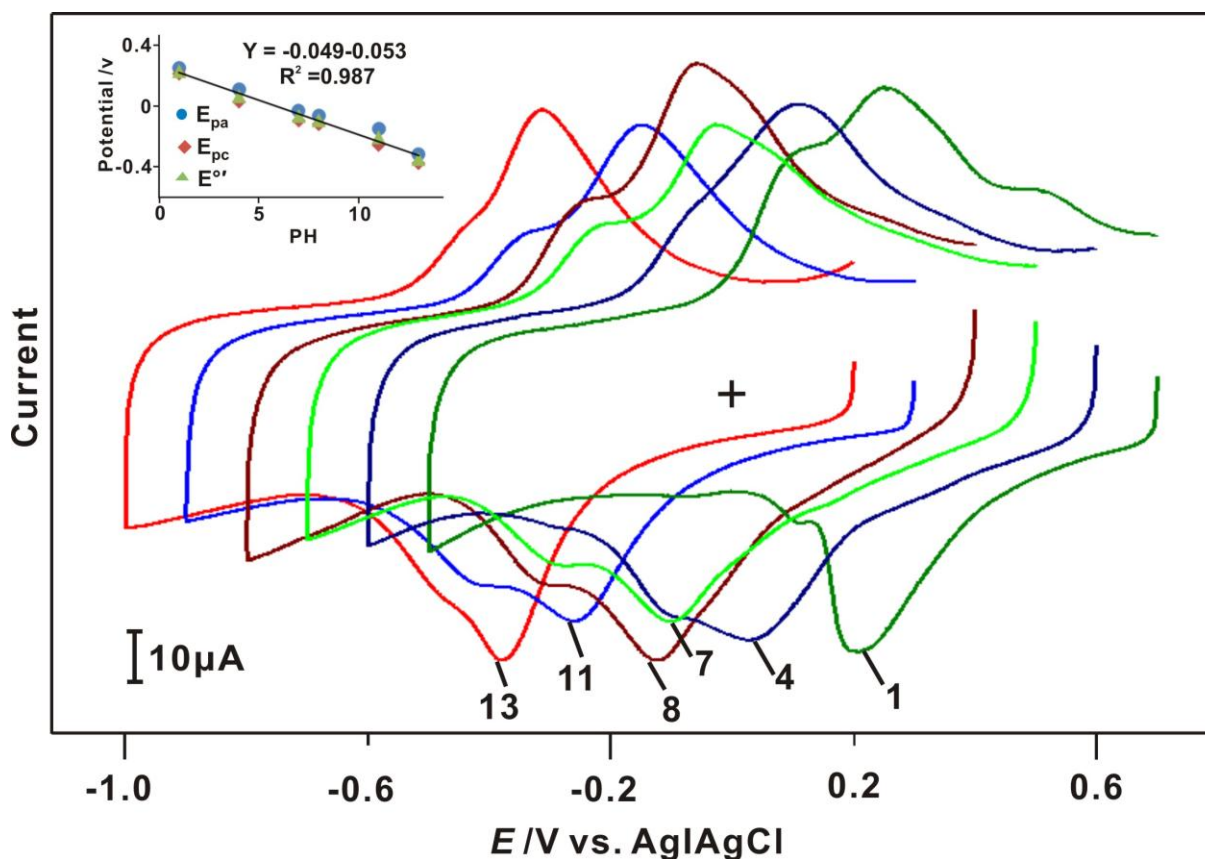


Figure 5. Cyclic voltammograms obtained at PTBO/ZrO₂/GCNT composite film modified GCE in deoxygenated different pH solutions: 1, 4, 7, 8, 11 and 13, respectively. Scan rate: 50 mV s⁻¹. Inset shows the influence of pH on E_{pa}, E_{pc} and E_{o'} values calculated for the redox couple II at PTBO/ZrO₂/GCNT composite film modified GCE.

With increase in pH of the solutions, both these redox peaks shifted towards the negative potential. On each occasion, before transferring the modified GCE to another buffer solution the film was washed several times with doubly distilled water. However, there was no considerable decrease in the peak currents, which validates the good stability of the nanocomposite film. Since the redox peak II was more obvious than redox peak I in the above mentioned pH range, as we discussed earlier the redox peak II corresponds to the polymer type reaction, we have presented the influence of pH on E_{pa} , E_{pc} and $E^{\circ'}$ values observed at redox peak II in Fig. 5 inset. It is apparent that both E_{pa} , E_{pc} and $E^{\circ'}$ values of the redox peak II exhibit a linear dependence on pH. The slope value is 49 mV/pH, which is close to the slope of 59 mV⁻¹ pH for equal number of proton and electron transfer processes. Thus the PTBO redox process involves an equal number of proton and electron transfer process. We also investigated the stability of nanocomposite film modified GCE in N₂ saturated 0.05 M pH 7 PBS by recording continuous CV potential scans in the potential range between +0.5 to -0.7 V at 50 mV s⁻¹. The peak currents (peak I and II) decreased slightly at the beginning, but no notable peak currents decrease and peak potential shifts were observed at the nanocomposite film after 200 consecutive CV potential scans, which shows its reasonable stability.

3.4. AFM studies

The surface morphology of various films has been investigated using AFM study.

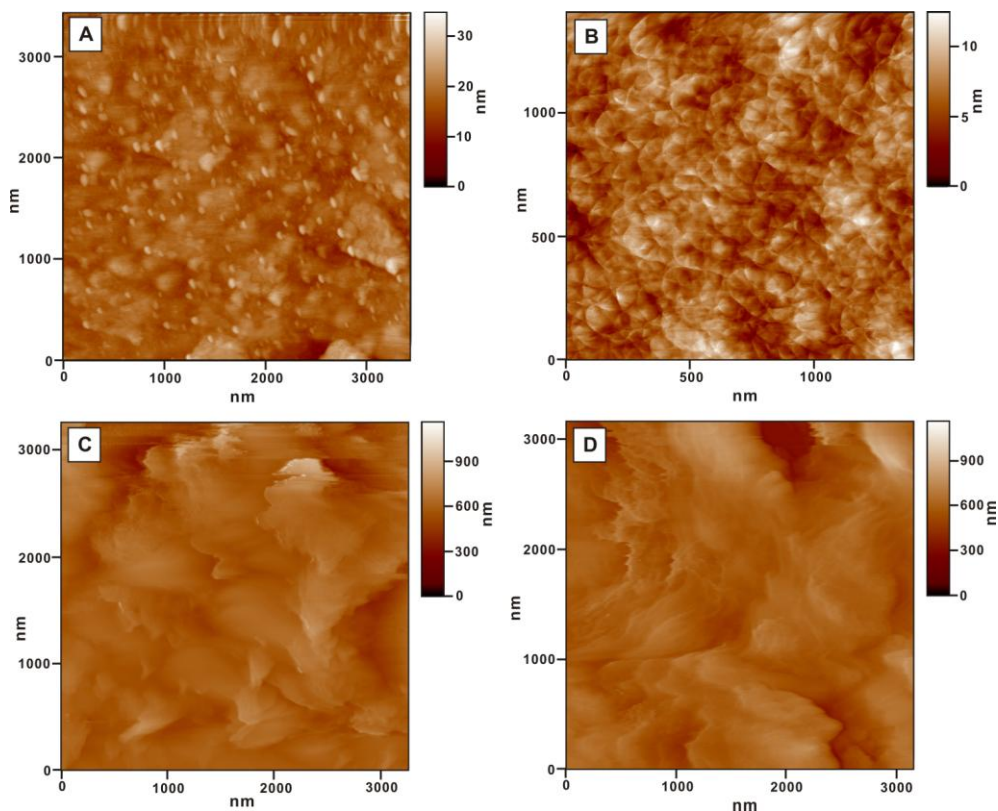


Figure 6. AFM images of (A) ZrO₂ NPs, (B) PTBO, (C) GCNT, and (D) PTBO/ZrO₂/GCNT film coated ITO electrodes.

Fig. 6 (A-D) shows the AFM images of ZrO_2 NPs, PTBO, GCNT and PTBO/ ZrO_2 /GCNT film coated indium tin oxide (ITO) electrodes. The AFM image of ZrO_2 NPs film shows numerous small, bright spherical shaped particles with an average size of 70–110 nm. Few slightly larger particles in the size range of 120-150 are also seen, which might have formed due to the union of two or more ZrO_2 nanoparticles. The height of the deposited ZrO_2 NPs is 30 nm, which shows its thin surface morphology. Whereas the AFM image of PTBO film surface displays wrinkle structures with numerous foldings. Compared with ZrO_2 NPs, PTBO film possesses very thin surface morphology which is evident from the smaller film height value of 10 nm. In the AFM image of GCNT film, CNTs are not clearly seen, since they are wrapped by a thick layer of gelatin.

The AFM image of PTBO/ ZrO_2 /GCNT revealed its thick surface morphology. The strong electrostatic interactions help the PTBO to attach firmly at the ZrO_2 NPs/GCNT surface, which avoids the leaching of PTBO from the composite film.

3.5. Electrocatalytic H_2O_2 reduction studies

Exposure to excess amount of H_2O_2 is highly dangerous and its can causes serious effects, hence H_2O_2 monitoring is essential for human welfare. So far, metal nanoparticles [34-36], metal oxides [37], conducting polymers [38], MWCNT-conducting polymers [39] and hexacyanoferrate film [40] modified electrodes have been successfully employed for H_2O_2 detection.

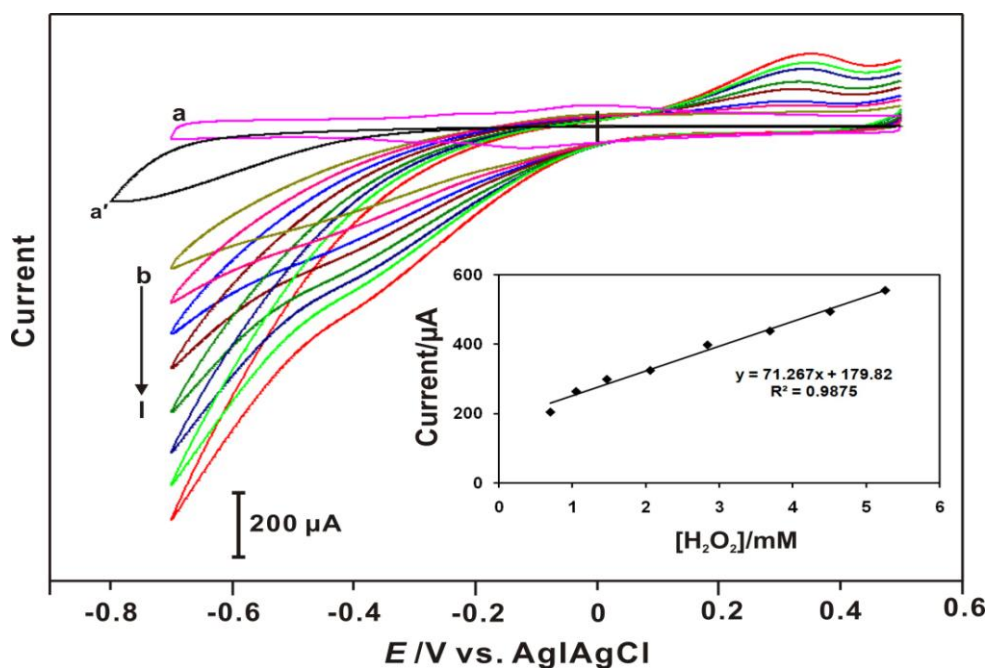


Figure 7. Cyclic voltammograms obtained at PTBO/ ZrO_2 /GCNT nanocomposite film modified GCE at the scan rate of 50 mV s^{-1} in the absence (a) and presence of: (b) 0.7, (c) 1.05, (d) 1.47, (e) 2.06, (f) 2.84, (g) 3.69, (h) 4.51 and (i) 5.26 mM H_2O_2 . Supporting electrolyte is N_2 saturated 0.05 M pH 7 PBS. Inset is the plot of cathodic peak current vs. $[\text{H}_2\text{O}_2]$. (a') cyclic voltammogram obtained at bare GCE in the presence of 5.26 mM H_2O_2 at similar conditions.

In this study, the electrocatalytic activity of the PTBO/ZrO₂/GCNT nanocomposite film has been investigated in N₂ saturated 0.05 M pH 7 PBS. Fig. 7 (a) shows the cyclic voltammogram obtained at PTBO/ZrO₂/GCNT/GCE in the absence of H₂O₂. The curves shown in fig. 7 (b-i) represents the electrocatalytic responses observed at the nanocomposite film modified GCE for various H₂O₂ concentration additions.

In the presence of 0.7 mM of H₂O₂, the electrocatalytic H₂O₂ reduction peak current starts at -0.1 V and an enhanced well-defined reduction peak is observed at -0.43 V. Since then, the reduction peak current gradually increases with increase in H₂O₂ concentration additions ((Fig. 7 (b-i)). The composite film shows promising electrocatalytic activity towards H₂O₂, which could be ascribed to the synergistic effect of PTBO/ZrO₂/GCNT nanocomposite for H₂O₂ as well as the ability of PTBO to mediate the H₂O₂ electrocatalytic reduction process. On the other hand, no catalytic H₂O₂ reduction peak was observed at bare/GCE even in the presence of 5.26 mM of H₂O₂, indicating that bare/GCE has no catalytic activity for H₂O₂ (see curve (a')). Compared with bare/GCE, PTBO/ZrO₂/GCNT/GCE decreased the H₂O₂ reduction over potential, validating the excellent electrocatalytic activity of the nanocomposite film.

The inset in Fig. 7 shows the calibration plot of I_{pc} vs. added H₂O₂ concentrations. The linear regression equation is $I (\mu\text{A}) = 71.267 C (\text{mM}) + 179.82$, $R^2 = 0.9875$. From this calibration plot, the linear concentration range and sensitivity values are obtained as 1.05–5.26 mM, and 0.902 $\mu\text{A } \mu\text{M}^{-1} \text{cm}^{-2}$, respectively.

Fig. 8 (a-d) shows the cyclic voltammograms obtained at various films modified GCEs in the presence of 5.26 mM of H₂O₂. GCNT modified GCE exhibits no significant electrocatalytic activity towards H₂O₂.

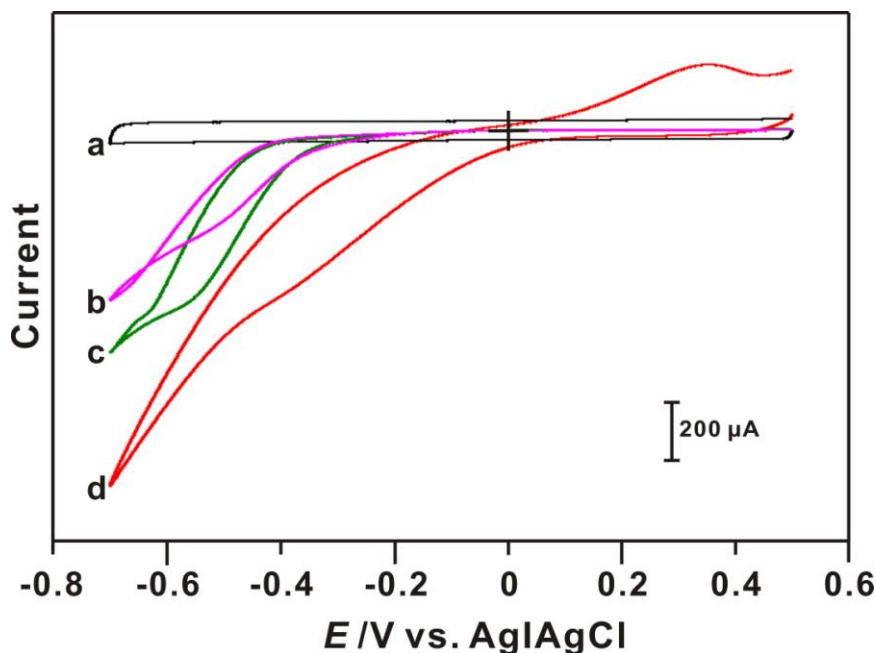


Figure 8. Cyclic voltammograms obtained at (a) GCNT, (b) PTBO, (c) PTBO/ZrO₂, and (d) PTBO/ZrO₂/GCNT nanocomposite film modified GCE at the scan rate of 50 mV s⁻¹ in the presence of 5.26 mM H₂O₂. Supporting electrolyte is N₂ saturated 0.05 M pH 7 PBS.

On the other hand, PTBO and PTBO/ZrO₂ film modified GCEs exhibit sharp electrocatalytic reduction peaks at -0.6 V and -0.63 V for 5.26 mM of H₂O₂. However, PTBO/ZrO₂/GCNT/GCE nanocomposite film modified GCE exhibits more enhanced H₂O₂ reduction peak at a low reduction potential of -0.37 V, which is 230 mV and 260 mV lower than the H₂O₂ reduction potentials observed at PTBO and PTBO/ZrO₂ modified GCEs. The proposed nanocomposite film thus exhibits good electrocatalytic activity towards H₂O₂ at low over potential, which could be ascribed to the ability of the strongly attached PTBO molecules to mediate the H₂O₂ reduction process.

3.6. Amperometric determination of H₂O₂ at various film modified rotating disc GCEs

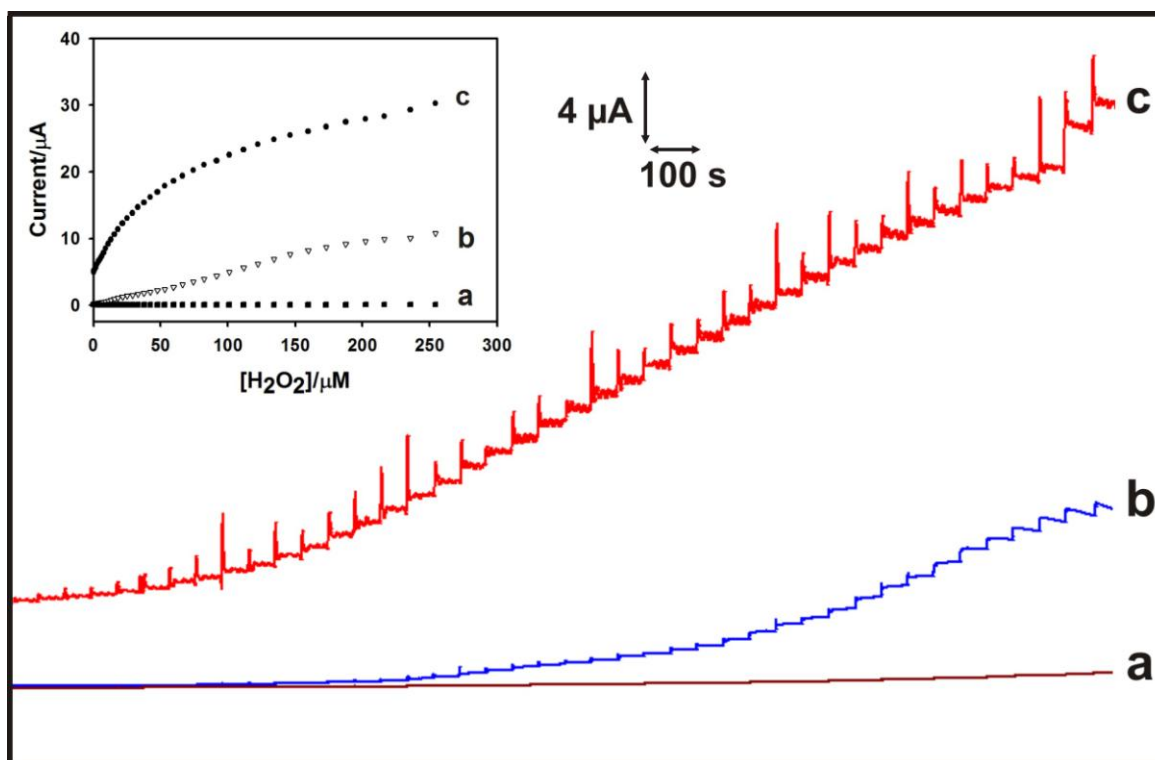


Figure 9. Amperometric *i-t* responses at (a) bare, (b) PTBO and PTBO/ZrO₂/GCNT film modified rotating disc GCEs upon successive additions of 0.03 μM to 0.25 mM H₂O₂ into continuously stirred N₂ saturated 0.05 M pH 7 PBS. Applied potential: -0.15 V; Rotation rate: 900 RPM. The inset plot shows the linear dependence of response currents on [H₂O₂]/μM.

Fig. 9 shows the amperometric *i-t* curves recorded at bare, PTBO and PTBO/ZrO₂/GCNT film modified rotating disc GCEs upon various H₂O₂ concentration additions in N₂ saturated 0.05 M pH 7 PBS. The electrode potential was kept constant at -0.15 V. For every 50 s, aliquots of H₂O₂ concentrations were successively injected into the supporting electrolyte solution. Among all the above mentioned rotating GCEs, PTBO/ZrO₂/GCNT film modified rotating GCE shows rapid, well-defined amperometric response with maximum response current towards each H₂O₂ concentration additions. The response time at the composite film is 5 s, which validates the fast electrocatalytic reduction

process occurring at this electrode surface. The linear dependence of amperometric response currents observed at various films upon different H_2O_2 concentrations is shown in fig. 9 inset. For the nanocomposite film, the linear regression equation is expressed as $I (\mu\text{A}) = 0.1062 C (\text{mM}) + 19.741$, $R^2 = 0.9898$. The linear H_2O_2 concentration range, correlation coefficient and the sensitivity values are calculated as $0.05 \text{ mM} - 0.25 \text{ mM } \text{H}_2\text{O}_2$, 0.9898 and $82.13 \mu\text{A } \mu\text{M}^{-1} \text{ cm}^2$, respectively. Satisfactory amperometric H_2O_2 quantification results achieved at the PTBO/ ZrO_2 /GCNT film in this study could be attributed to the good stability of nanocomposite film and ability of the strongly attached PTBO molecules to mediate the H_2O_2 reduction process.

3.7 Real sample analysis

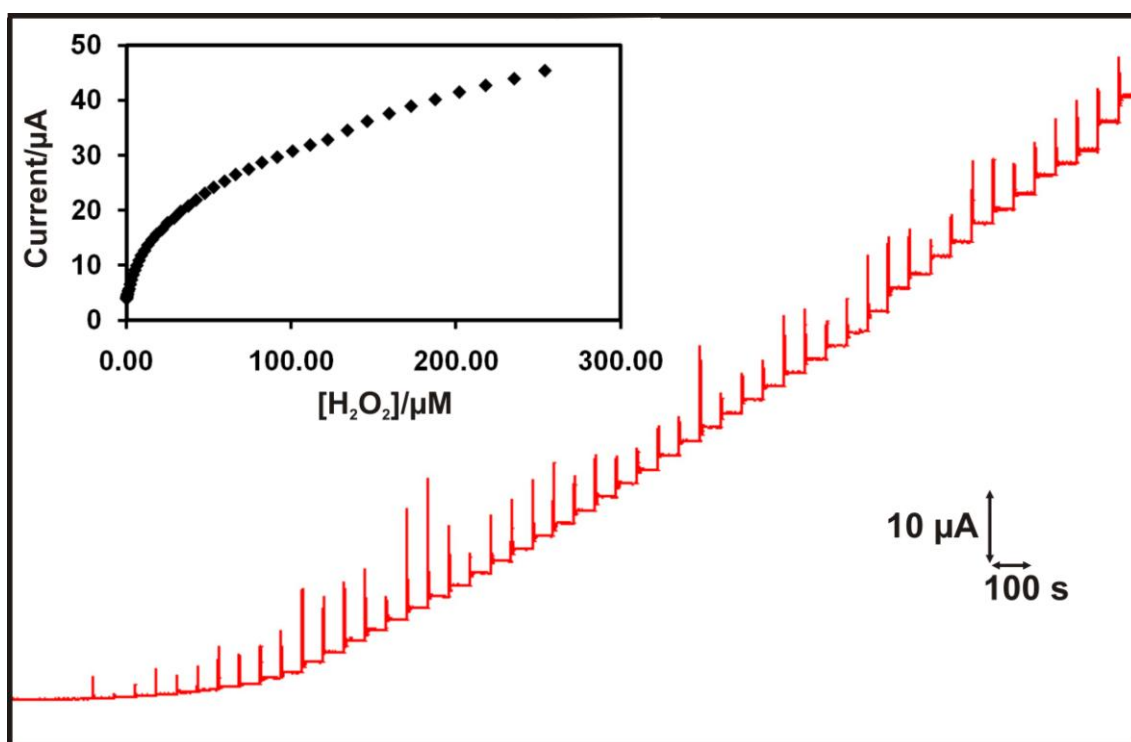


Figure 10. Amperometric *i-t* response at PTBO/ ZrO_2 /GCNT film modified rotating disc GCE upon successive additions of $0.03 \mu\text{M}$ to 0.25 mM of H_2O_2 containing antiseptic solutions into continuously stirred N_2 saturated 0.05 M pH 7 PBS. Applied potential: -0.15 V ; Rotation rate: 900 RPM . The inset plot shows the linear dependence of response currents on $[\text{H}_2\text{O}_2]/\mu\text{M}$.

The practical applicability of PTBO/ ZrO_2 /GCNT composite film modified rotating disc GCE has been investigated through real sample analysis using amperometric *i-t* curve studies. Commercially available antiseptic solution containing 30 % H_2O_2 was purchased from a local drug store in Taipei, Taiwan. Further dilutions were made using 0.05 M pH 7 PBS. The working electrode potential was kept constant at -0.15 V . From fig. 9, it is clear that PTBO/ ZrO_2 /GCNT composite film modified rotating GCE exhibits well defined amperometric responses towards H_2O_2 in the linear concentration range between $0.03 \mu\text{M}$ and 0.25 mM , which shows its good practical applicability.

4. CONCLUSIONS

In the present study, we report the preparation and characterization of novel PTBO/ZrO₂/GCNT nanocomposite film for the amperometric determination of H₂O₂. The electrochemically synthesized ZrO₂ NPs are in the size range of 70-110 nm. CV results revealed that TBO polymerization occurs more efficiently at ZrO₂/GCNT composite matrix. The presence of GCNT in the composite film provides good conductivity and stability. The fabricated PTBO/ZrO₂/GCNT composite film exhibits promising electrocatalytic activity, rapid response towards H₂O₂ at physiological pH.

ACKNOWLEDGEMENT

This work was supported by the National Science Council and the Ministry of Education of Taiwan (Republic of China).

References

1. P. A. Prakash, U. Yogeswaran, S. M. Chen, *Talanta*, **78** (2009) 1414.
2. A. Mikolajczuk, A. Borodzinski, L. Stobinski, P. Kedzierzawski, B. Lesiak, L. Kover, J. Toth, H.M. Lin, *Phys. Status Solidi B*, **247** (2010) 3063.
3. T. Sawatsuk, A. Chindaduang, C.S. kung, S. Pratontep, G. Tumcharern, *Diamond Relat. Mater.*, **18** (2009) 524.
4. S. Campidelli, C. Klumpp, A. Bianco, D.M. Guldi, M. Prato, *J. Phys. Org. Chem.*, **19** (2006) 531.
5. G. Gruner, *Anal Bioanal Chem.*, **384** (2006) 322.
6. H. Lee, M. Lee, S. Namgung, S. Hong, *Nano Lett.*, **4** (2010) 7612.
7. S. Costa, E.B. Palen, A. Bachmatiuk, M.H. Rummeli, T. Gemming, R.J. Kalenczuk, *Phys. Stat. Sol. (b)*, **244** (2007) 4315.
8. U. Yogeswaran, S. Thiagarajan, S.M. Chen, *Anal. Biochem.* **365** (2007) 122.
9. W.D. Zhang, B. Xu, L.C. Jiang, *J. Mater. Chem.*, **20** (2010) 6383.
10. L. Agui, M. Eguilaz, C.P. Farfal, P.Y. Seden, J.M. Pingarron, *Electroanal.* **21** (2009) 386.
11. B. Gupta, S. Singh, S. Mohan, R. Prakash, *Biosensors*, Edtd. by P.A. Serra, Intech, Croatia, (2010) 302.
12. C. X. Cai, K. H. Xue, *Talanta*, **47** (1998) 1107.
13. Y. Chen, J. Yuan, X. Wang, C. Tian, *Anal. Sci.*, **20** (2004) 1725.
14. S. A. Kumar, S. M. Chen, *Electroanal.* **19** (2007) 1952.
15. J. Zeng, W. Wei, L. Wu, X. Liu, K. Liu, Y. Li, *J. Electroanal. Chem.*, **595** (2006) 152.
16. D.J. Guo, X.P. Qiu, W.T. Zhu, L.Q. Chen, *Appl. Catal., B*, **89** (2009) 597.
17. Y. Shan, L. Gao, *Nanotechnol.*, **16** (2005) 625.
18. S.A. Steiner, T.F. Baumann, B.C. Bayer, R. Blume, M.A. Worsley, W.J. MoberlyChan, E.L. Shaw, R. Schlogl, A.J. Hart, S. Hofmann, B.L. Wardle, *J. Am. Chem. Soc.*, **2009** (131) 12144.
19. B. Liu, J. Hu, J.S. Foord, *Electrochem. Solid-State Lett.*, **14** (2011) D20.
20. Z. Tong, R. Yuan, Y. Chai, S. Chen, Y. Xie, *Biotechnol. Lett.*, **29** (2007) 791.
21. G. Liu, Y. Lin, *Anal. Chem.*, **77**(2005) 5894.
22. I.Slesak, M. Libik, B. Karpinska, S. Karpinski, and Z. Miszalski, *Acta Biochim. Pol.*, **54** (2007) 39.
23. C. K. Yeh, H. Wu, T. Chen, *J. Hazard. Mater.*, **96** (2003) 29.
24. R. J. Weston, *Food Chem.*, **71** (2000) 235.
25. D. B. Moore and D. S. Argyropoulos, *Anal. Chem.*, **71** (1999) 109.
26. T. Tatsuma, Y. Okawa, and T. Watanabe, *Anal. Chem.*, **61** (1989) 2352.

27. A.V. Jackson and C. N. Hewitt, *Atmos. Environ.*, 30 (1996) 819.
28. C. Xu and Z. Zhang, *Anal. Sci.*, 17 (2001) 1449.
29. C. Matsubara, K. Kudo, T. Kawashita and K. Takamura, *Anal. Chem.*, 57 (1985) 1107.
30. A.P. Periasamy, Y. J. Chang, S.M. Chen, *Bioelectrochem.* 80 (2011) 114.
31. Y. Jia, C. Duran, Y. Hotta, K. Sato, K. Watari, *J. Colloid Interface Sci.*, 291 (2005) 292.
32. W. Zheng, Y.F. Zheng, *Electrochem. Commun.*, 9 (2007) 1619.
33. Y. Wang, S. Hu, *Biosens. Bioelectron.*, 22 (2006) 10.
34. M. Rajkumar, S. Thiagarajan, S. M. Chen, *J. Appl. Electrochem.* 41 (2011) 663.
35. S. A. Kumar, P. H. Lo, S.M. Chen, *J. Electrochem.Soc.*, 156 (2009) E118-E123.
36. M.H. Chiu, A.S. Kumar, S. Sornambikai, P.Y. Chen, Y. Shih, J.M. Zen, *Int. J. Electrochem. Sci.*, 6 (2011) 2352 - 2365.
37. A.P. Periasamy, S.W. Ting, S.M. Chen, *Int. J. Electrochem. Sci.*, 6 (2011) 2688-2709.
38. H.W. Siao, S.M. Chen, K.C. Lin, *J. Solid State Electrochem.* 15(2011) 1121–1128.
39. K.C. Lin, T.H. Tsai, S.M. Chen, *Biosens. Bioelectron.* 26 (2010) 608–614.
40. R.C. Pena, J.C.M. Gamboa, M. Bertotti, T.R.L.C. Paixao, *Int. J. Electrochem. Sci.*, 6 (2011) 394-403.